Neuromodulation: Technology at the Neural Interface

Received: June 30, 2025 Revised: August 5, 2025 Accepted: August 20, 2025

https://doi.org/10.1016/j.neurom.2025.08.412

Correlation of Electrical Impedance and Evoked Potentials With Properties of the Electrode Interface Using in Situ Block-Face Imaging of the Rat Pelvic Nerve

Sophie C. Payne, PhD[1,2]; Christopher Bowman, BSc (Hons)[1]; Janet R. Keast, PhD[3]; Ella P. Trang, BSc (Hons)[1,2]; Peregrine B. Osborne, PhD[3]; James B. Fallon, PhD[1,2,4]

ABSTRACT

Background: Electrical stimulation is an emerging therapy for urologic disorders. The interface between electrode and neural tissue is a critical region of interest given it affects thresholds of neural activation. Measures of electrode impedance are used clinically to estimate tissue fibrosis at the interface; however, the relationship between impedance and fibrosis is not well defined.

Objective: This study aimed to assess the relationship between interface tissue fibrosis and nerve distance from electrode surface with measurements of impedance and evoked thresholds using a chronic model of visceral nerve implantation.

Materials and Methods: An extraneural four-platinum electrode array was implanted on the rat ($N = 14$) pelvic nerve and measured common ground impedance, transimpedance, and electrically evoked neural thresholds during two weeks of implantation. A novel serial block-face staining and imaging technique was used to assess the electrode-nerve interface in situ.

Results: Analysis revealed no significant correlations between impedance or neural threshold and fibrotic tissue area ($p > 0.05$). Proximal electrodes 1 and 2 were significantly further away from neural tissue than were distal electrodes 3 and 4 ($p < 0.011$). Despite this, there were no differences in neural thresholds among electrode configurations ($p > 0.05$).

Conclusion: Measurements of electrode impedance and neural thresholds indicate the presence but not the absolute amount of interface tissue fibrosis. Understanding the dynamics of the nerve–electrode interface is essential for designing suitable peripheral nerve electrode arrays and informing on stimulation parameters to advance the future clinical use of pelvic nerve stimulation as a neuromodulation therapy in urologic disorders.

Keywords: Chronic in vivo recording, electrical impedance, grinding histology method, peripheral nerve interface

INTRODUCTION

Electrical stimulation of the peripheral nervous system is used clinically to treat a wide range of diseases including epilepsy, depression, migraine, obesity, and fecal and urinary incontinence.[1,2] However, despite the success of stimulating the autonomic nervous system to treat disease, clinical trials are often affected by high variability in the response of patients, with little understanding of ways to improve the outcome.[3] The interface between an extraneural electrode and multifascicle peripheral autonomic nerves is a critical region that significantly affects the thresholds of activation and the ability to record an evoked

Address correspondence to: James B. Fallon, PhD, 35 Victoria Parade, Fitzroy 3065, Victoria, Australia. Email: jfallon@bionicsinstitute.org

[1] Bionics Institute, Fitzroy, Australia;
[2] Medical Bionics Department, University of Melbourne, Melbourne, Australia;
[3] Department of Anatomy and Physiology, University of Melbourne, Melbourne, Australia; and
[4] Department of Otolaryngology, University of Melbourne, Melbourne, Australia

For more information on author guidelines, an explanation of our peer review process, and conflict of interest informed consent policies, please see the journal's Guide for Authors.

Source(s) of financial support: Research reported in this publication was supported by the National Institutes of Health, Office of the Director, Stimulating Peripheral Activity to Relieve Conditions (SPARC) Program, Award Number OT2OD023872 (JRK, PBO, and JBF). The content is solely the responsibility of the authors and does not necessarily represent the official views of the National Institutes of Health. The Bionics Institute also acknowledges the support they receive from the Victorian Government through its Operational Infrastructural Support Program.

response. Variations in the electrode-nerve interface likely contribute to the variability in the delivery of treatment,[4] the most notable components being the growth of fibrotic tissue and the electrode–nerve distance.[5] Characterization of the conditions within the interface that affect efficacy of stimulation is important to improve understanding of the causes of interpatient variability in addition to suggesting refinements in electrode array designs and stimulation strategies.[3,6]

Our own rat[7–9] and sheep[10] vagus nerve long-term implantation studies consistently report an initial increase in electrode common ground impedance over two weeks, after which impedance values stabilize. Furthermore, impedance values increase over two weeks after long-term implantation on the pelvic nerve of male rats, with no further changes to impedance observed at eight weeks.[11] Similar changes are reported during long-term implantation of cervical vagus nerve implantation in rats,[12] surface brain stimulation electrodes (Responsive Neurostimulation System [RNS®]),[13] and deep brain stimulation electrodes in humans.[14] Higher impedances can be problematic for safe delivery of electrical charge, with the higher levels of voltage potentially leading to irreversible electrochemical reactions at the interface, the formation of gas bubbles, ionic changes, and pH shifts that are harmful to tissue and the electrode.[15,16] There is a general consensus that increases in electrical impedance during long-term implantation are a consequence of the growth of epineural fibrosis within the electrode-nerve interface,[17–19] which occurs owing to an inflammatory foreign body response to the extraneural cuff electrode array.[20] Electrode impedance also may fluctuate owing to increases in the effective surface area resulting from high charge stimulation,[21] or from electrode biofouling, which naturally occurs from the accumulation of biological matter (protein deposits, cells, etc) at the electrode-electrolyte interface during long-term implantation to reduce the active electrode area.[22,23]

Despite the complex interplay between changes in electrode surface and tissue response, measurements of transimpedance and common ground impedance are routinely used in the clinic as measures of the electrode–nerve interface.[6] Common ground impedance is a simple measure of the peak voltage at the end of the active phase of stimulation on the stimulating electrode and compared with all other electrodes within the array. Although this measure is simple to perform, its interpretation is complicated by the polarization of the stimulating electrode. Transimpedance measures the voltage decay along the length of the electrode array on unstimulated electrodes, eliminating the issue of polarization of the stimulating electrode. Although both methods are used clinically in cochlear implantation technology,[24] the use of common ground impedance and transimpedance as a tool for informing on interface tissue fibrosis for autonomic nerve electrode arrays is less well studied and comprises the first aim of this study.

Significant advances have recently been made in computational modeling of electrical stimulation and recording from autonomic nerves.[5,25–27] Surrogate fiber models that simulate spatiotemporal responses to many peripheral nerve stimulation protocols have been built based on anatomical and physiologic properties of axons in addition to the dynamic properties of the cuff electrode array.[26] However, in most surrogate fiber models, there is a paucity of data that account for the effects of the interface tissue fibrosis and electrode–nerve distance on evoked neural thresholds.[26] The electrode–nerve interface significantly affects both the efficacy of stimulation delivered and the quality of recording.[5] Visceral nerves, such as the rat pelvic nerve (rodent homolog of human pelvic splanchnic nerves), are small, fragile, multifascicular, and constrained within a loose epineurium structure,[28,29] and present a significant challenge for the design of electrode–nerve interfaces in peripheral nerve arrays.[30] The recruitment profile of different fascicles in the pelvic nerve will likely be affected by the fascicle-electrode distance, which has functional implications given studies show different fascicles in another autonomic nerve (ie, the vagus nerve) can have different physiologic roles.[26] This could have major implications for efficacy in pelvic nerve stimulation studies as a future neuromodulation therapy for neuro-urologic and other pelvic functional disorders.[11,31,32] As such, the second aim of this study is to assess the correlation between stimulation threshold of evoked neural responses and interface tissue fibrosis. A final aim is to assess ways the distance of the pelvic nerve from stimulating and recording electrodes affects neural thresholds.

In this study, we performed a long-term implantation of a planar extraneural four-electrode array on the pelvic nerve of rats, which is an exemplar mutifascicle visceral (autonomic) nerve that has gained recent interest as a potential target site for the treatment of urologic disorders.[11,31,32] To assess the electrode–nerve interface after two weeks of long-term implantation, we optimized and adapted a novel histologic block face imaging technique,[33,34] which involves sequential grinding and block-face imaging to visualize in situ the interface of the four platinum electrodes with the nerve. Common ground impedance, transimpedance, and evoked potential measurements were correlated with the thickness of fibrotic tissue buildup within the electrode-nerve interface. Correlations between stimulation thresholds and the fascicle distance from the stimulating and recording electrodes also were assessed. The resulting understanding of the impact of the electrode-nerve distance and fibrotic tissue buildup will likely inform future electrode array designs to improve efficacy of stimulation and recording.

MATERIALS AND METHODS

Peripheral Nerve Electrode Array Design

Electrode arrays were manufactured in-house (Bionics Institute, Victoria, Australia). As previously described,[11] the array had four platinum (99.95%) electrodes (E1–E4) with an exposed recessed surface area of 0.36 mm^2 (1.8 mm × 0.2 mm) contained within medical grade silicone. Adjacent electrode pairs were 0.75 mm apart (center to center) and electrode pairs were 3.25 mm apart (center to center) (Fig. 1a). A Dacron embedded silicon tab surrounded the array to allow securement to underlying subcutaneous tissue. Insulated platinum/iridium (90/10, 50 μm diameter) wires were welded to each electrode and formed a helical cable that traversed to a percutaneous connector. A subcutaneous ring electrode on the cable acted as a return. The percutaneous pedestal was secured to the lumbar aspect of the rat using a Dacron embedded silicon tab.[35]

Animals and Anesthesia

A total of 30 male Sprague-Dawley rats (eight–nine weeks at the start of the experiment, Animal Resource Centre, Western Australia) were used. Of these 30 rats, $n = 7$ were excluded owing to having a broken or shorted electrode; $n = 1$ rat died during surgery, and $n = 2$ rats were excluded owing to failure of the

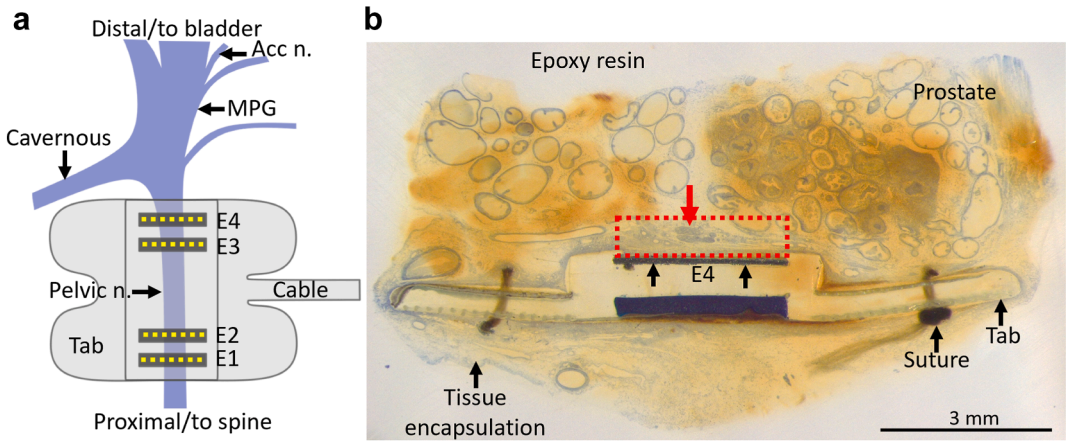

Figure 1. Pelvic nerve anatomy and histologic processing of the interface in situ. a. Schematic diagram indicates the anatomy of the left major pelvic ganglion and its associated nerves, that is, the pelvic, cavernous, and accessory nerves. The electrode array had two pairs of platinum electrodes. The location of the electrode array at the time of surgery is indicated in panel a. Electrodes E1–E2 were positioned proximal or closest to the spinal cord, whereas E3–E4 were positioned distal or closest to the end organ, that is, the bladder. Images of the block face were obtained at each electrode (E1, E2, E3, E4, indicated by yellow dotted lines). The silicon-embedded "tab" was anchored to connective tissue overlying the prostate gland using sutures. b. Prostate and associated neural tissue (indicated by red dotted box) and implanted electrode array were dissected together and processed in situ. A large blood vessel typically associated with the pelvic nerve is indicated by the red arrow. The black arrows indicate the electrode interface from electrode 4 (E4). The tissue-electrode complex was processed, double-embedded in an epoxy resin mixture, and stained with Toluidine blue for block-face imaging. Scale bar for panel b represents 3 mm. [Color figure can be viewed at www.neuromodulationjournal.org]

bladder cannula required for other experimental aspects and were euthanized early. As such, experimental procedures and data are reported from $N = 20$ rats in this study.

All animal procedures were approved by St Vincent's Hospital Animal Ethics Committee and complied with the Australian Code for the Care and Use of Animals for Scientific Purposes (National Health and Medical Research Council of Australia). After surgical implantation, rats were housed individually to prevent damage to the percutaneous pedestal, and environmental enrichment was provided. Rats were kept under a 12-hour light-dark cycle in a temperature-controlled room and allowed ad libitum access to food and water. Surgical procedures were conducted under isoflurane anesthesia (3% for induction, 1.5%–2% for maintenance in 1 L/min oxygen).

Analgesia (5 mg/kg carprofen, subcutaneous; buprenorphine 0.03 mg/kg, subcutaneous) and fluids (3 mL/100 g Hartman's Solution subcutaneous) were provided during surgery. For the first three days after surgery, animals were given fluids twice a day (3 mL/100 g Hartman's Solution) to help prevent the development of cystitis after bladder catheterization surgery. At the completion of the experiment, animals were euthanized (300 mg/kg, Lethabarb, intraperitoneal).

Surgical Procedures

The pelvic nerve implantation surgery is described in.[11,36] In brief, animals were anaesthetized, and under aseptic conditions, the abdominal cavity was opened and the left pelvic nerve exposed and identified. The four electrodes were carefully aligned perpendicular to the pelvic nerve and the array secured to underlying prostate tissue using sutures (7'0, Ethicon). Care was taken to avoid mechanical damage to neural tissues during implantation. The abdominal cavity was sutured closed, and the percutaneous pedestal of the array was sutured to the dorsal-lumbar aspect of the spine and the skin closed around it.

Impedance Measurements and Electrophysiological Recording

Impedance (transimpedance and common ground impedance), electrically evoked compound action potentials (ECAPs), and physiologically evoked neural responses were measured.

Impedance Testing

Common Ground. The functionality of the implanted electrodes was evaluated at surgery and at one and two weeks after implantation by measuring the common ground impedance of electrodes. To measure the common ground impedance of an electrode, a symmetric biphasic current pulse (100 pulses per second, 100 μA, 100 μs per phase, 50 μs interphase gap) was delivered to each electrode, with all other electrodes shorted together serving as the return electrode, using a custom simulator made in-house (Bionics Institute).[37] The peak voltage transient recorded at the end of the first phase used to calculate the total impedance (ohms law = voltage/current).[37,38] For example, a common ground impedance measurement of 10 kΩ for "E1" informs on the impedance of the stimulating electrode (E1) compared with all other electrodes (E2–E4).

Transimpedance. A transimpedance matrix was generated by passing a symmetric biphasic current pulse (250 pulses per second, 25 μs per phase, 8-μs interphase gap, 106.5 μA) between the electrode of interest and a remote return electrode and measuring the voltage on all other electrodes in the array at the end of the first phase using a Nucleus CI24 cochlear implant and Nucleus ESPrit 3G speech processor[39] (Cochlear, Englewood, CO). The voltage is expected to decrease as the distance between stimulating and recording electrodes increases. The result of the measurement is a matrix of 4 × 4 (transimpedances). For display and statistical analysis, the transimpedance measurement of the electrode of interest was measured from the closest adjacent electrode. For example, the transimpedance measurement for E1 was measured from E2, whereas measurements for E3 were taken from E4 (Table 1).

Table 1. Schematic Diagram of the 4 × 4 Transimpedance Matrix Generated for the Four-Planar Pt Electrode Array.

	R1	R2	R3	R4
S1	X	E1		
S2	E2	X		
S3			X	E3
S4			E4	X

The transimpedance measurement of the electrode of interest was measured from the closest adjacent electrode. For example, impedance of E1 was measured from S1R2; E2 impedance was measured from S2R1; E3 impedance was measured from S3R4; and E4 impedance was measured from S4R3.

Electrically Evoked Compound Action Potentials. Similar to those previously described,[11,38] the thresholds of ECAPs were determined by stimulating with biphasic current pulses (100 μs; 10 Hz; 0–2 mA) and recording evoked activity (averaged over 50 stimuli and two repeats) using an isolated differential amplifier with an active probe (ISO-80, World Precision Instruments, FL). Recordings were sampled at a rate of 200 kHz and digitally filtered (300–5000-Hz band pass) using a data acquisition device (USB-6210, National Instruments, TX). The threshold of evoked neural responses was visualized using Igor Pro 9 software (WaveMetrics, Inc, Portland, OR) and defined as the minimum stimulus intensity producing a response amplitude above noise (≥0.1μV) in both repeat recordings. The threshold current level for this response was analyzed. If no response was recorded, data were coded as "300 CL," a level likely to be an underestimation of the real value.

Histology and Block Face Imaging

At two weeks after implantation surgery, animals were euthanized and perfused intracardially with saline (0.9% sodium chloride and 5000 IU/mL heparin), then fixative (10% neutral buffered formalin, pH 7.4). The entire electrode array and attached adjacent prostate tissue were dissected out as a whole specimen and postfixed (10% neutral buffered formalin, pH 7.4) overnight at 4 °C. After postfixing and thorough washing in phosphate buffered saline (pH 7.4), samples were dehydrated in ethanol for two days using serial concentrations progressing from 70% to 100%. Overnight immersion in acetone was used to clear the tissue. After 5 minutes drying in air, samples were immersed in an epoxy resin mixture (4:1 composition of epoxy resin and hardener, EpoTek 301 resin, Epotek 301 hardener, Epoxy Technology, MA) and a vacuum applied (4 minutes) to ensure full infiltration of the mixture and removal of air bubbles. To aid in the orientation of the block, a second embedding was performed by repeating the steps previously described. After appropriate orientation, blocks were re-embedded so that the electrode and adjacent tissue were perpendicular to the plane of sectioning (Fig. 1). The samples were placed in a holder (AccuStop, Struers, Copenhagen, Denmark) that was set to allow progressive removal of a specific block thickness (120 μm per step) using a grinding machine (Labopol-30, Struers, Copenhagen, Denmark). After every 120 μm, the surface was polished (with grinding paper) and stained with 1% Toluidine blue (8 minutes, Westlab, Victoria, Australia). Four levels through the block were imaged (Fig. 1b) to allow visualization of the pelvic nerve trajectory across the electrode array. Each level was at the location of an electrode (E1–E4, Fig. 1b). Representative light microscope images of Toluidine blue stained sections were taken using a Zeiss Axioplan II microscope (Carl Zeiss Microscopy, Jena, Germany) and AxioVision Software (Zeiss, New York, NY).

Histologic Analysis of Interface

Images were viewed and analyzed using FIJI / ImageJ software.[40] Key structures such as neural fascicles, the electrode, silicone mold, and fibrotic tissue response were identified as regions of interest (ROIs, Fig. 1b, 2a).

Fibrotic Tissue Area. The area of the fibrotic tissue response at the electrode interface was evaluated as in Figure 2a.

Putative Identification of the Pelvic Nerve. The pelvic nerve was defined as a collection of neural fascicles associated with a signature blood vessel that was typically embedded amongst the pelvic nerve fascicles.[29]

Pelvic Nerve Area. The pelvic nerve area was defined as the epineurium boundary and adjacent blood vessels embedded between fascicles.

Total Fascicle Area. The total fascicle area was defined as the total area of neural fascicle tissue. This measurement was distinct from the pelvic nerve area because it did not include blood vessels or space between fascicles and the epineurium boundary.

Fascicle to Electrode Distance. The centroid of each ROI was measured as x, y position, and the shortest distance between a neural ROI and the electrode ROI was calculated using the Euclidian distance between the centroids.

Statistics

Details of each statistical test are stated in the relevant results section. In brief, differences over time in impedance measurements and neural thresholds were tested using a one-way or two-way repeated measures (RM) analysis of variance (ANOVA) with appropriate post hoc tests, stated in the Results. A Pearson correlation test was used to correlate electrical impedance/ECAPs with interface tissue area, or neural thresholds with measurements of tissue thickness. Statistically significant differences were accepted as p-values <0.05, and GraphPad Prism 10 (GraphPad Software, Boston, MA) or Igor Pro 9 software used for all analysis.

RESULTS

Impedance and ECAPS as a Measure of Interface Tissue Fibrosis

Interface Fibrotic Tissue Area Across Electrode Array

The area of fibrotic tissue between the electrode surface and neural tissue was measured from block-face images (Fig. 2a, indicated by red dotted box; Fig. 2b). The four platinum electrodes in each array were numbered E1 and E2, which were proximal or closest to spinal cord, and E3 and E4, which were distal or closest to the major pelvic ganglia and bladder. The interface fibrotic tissue area (Fig. 2a, indicated by red dotted box) was similar across all electrodes (Fig. 2b). One-way RM ANOVA did not detect a significant difference in fibrotic tissue area across electrodes ($N = 12$ rats, $F_{(3,33)} = -2.10$; $p > 0.999$; E1: 0.18 ± 0.01 mm^2; E2: 0.19 ± 0.02 mm^2; E3: 0.16 ± 0.01 mm^2; E4: 0.15 ± 0.01 mm^2).

Changes in Common Ground Impedance During Long-Term Implantation

Common ground impedance (CG) was recorded immediately after surgery and after two weeks of implantation onto the pelvic nerve.

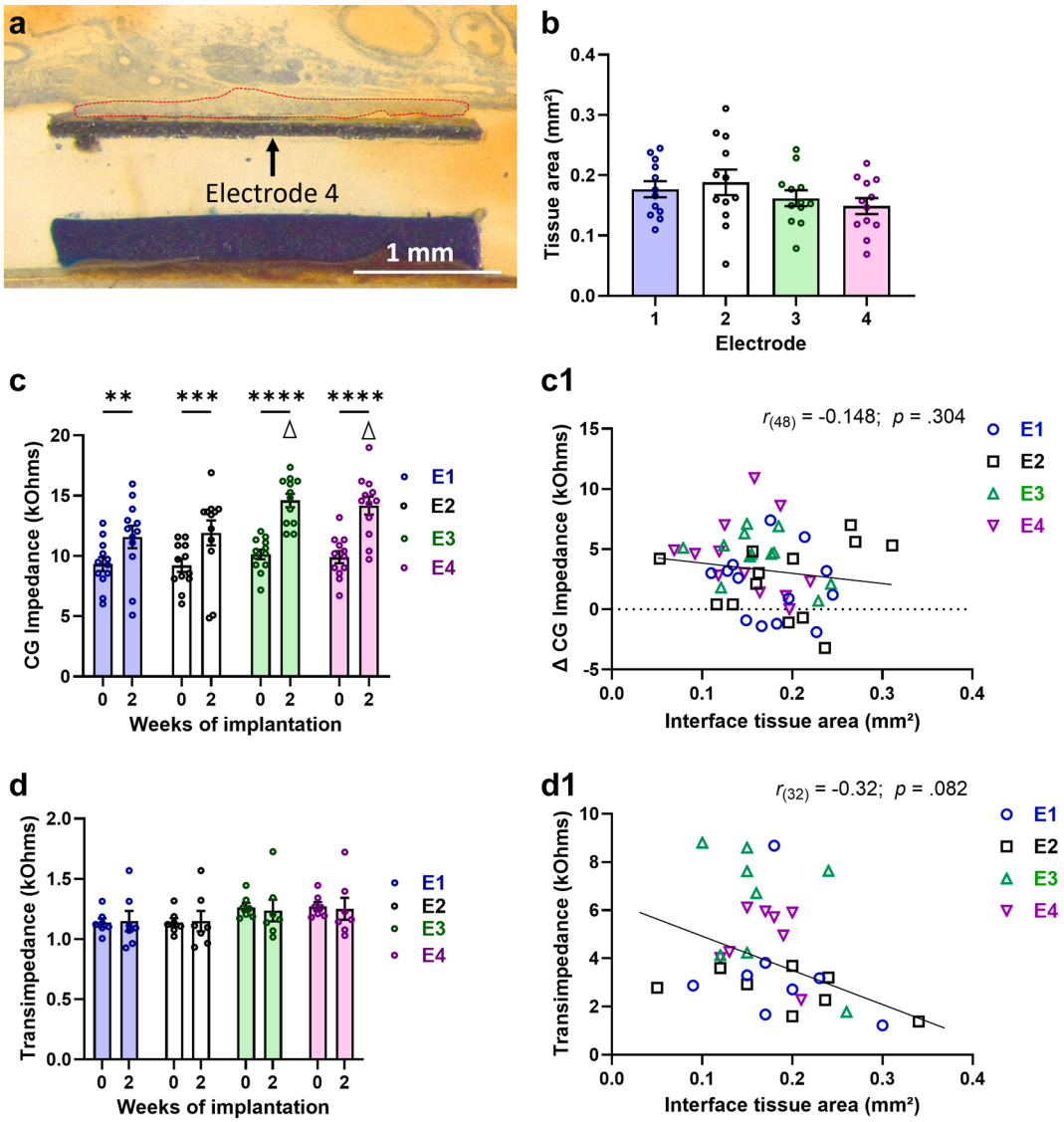

Figure 2. No correlation between electrical impedance and fibrotic tissue area within the interface after two weeks of pelvic nerve implantation. a. Image of epoxy-resin embedded Toluidine blue stained sample showing electrode 2 in situ implanted long term on the pelvic nerve and surrounding prostate tissues. T fibrotic tissue response (indicated by red dotted box) was measured and correlated with recordings of electrical impedance. b. Fibrotic tissue area at the interface was assessed across all electrodes (E1–E4). c. Graph shows CG impedance across electrodes 1 to 2 (E1–E4) at time of surgery (0 weeks) and two weeks after implantation. c1. Correlation between fibrotic tissue area and Δ CG impedance at two weeks after implantation. d. Graph shows transimpedance across electrodes 1 to 2 (E1–E4) at time of surgery (0 weeks) and two weeks after implantation. d1. Correlation between fibrotic tissue area and transimpedance at two weeks after implantation. Scale bar in panel a represents 1 mm. Data in b, c, and d show mean ± SEM, and symbols are values from individual rats. In panel b, differences in fibrotic tissue area between electrodes (n = 12) were analyzed using RM one-way ANOVA. In panels c and d, RM two-way ANOVA and Sidak's post hoc test were performed to analyze the effect of Time × Electrode on electrical impedance. Significant differences across time are indicated as * $p < 0.05$; ** $p < 0.01$; *** $p < 0.001$; **** $p < 0.0001$. Differences between electrode pairs E3 and E4 and E1 and E2 are indicated by Δ. In panels c1 to d1, the correlation between fibrotic tissue area and Δ CG impedance (net difference between impedance at 0 and two weeks, c1) or transimpedance (d1) was assessed using Pearson's correlation and significance accepted as $p < 0.05$. [Color figure can be viewed at www.neuromodulationjournal.org]

Data were only analyzed in animals when all electrodes (E1–E4, N = 48) remained functional with no open or short circuits. As expected, CG impedances were similar for all electrodes immediately after surgery and increased during the two weeks of implantation (Fig. 2c). A two-way (Time × Electrode) RM ANOVA indicated a significant interaction between Time × Electrode ($F_{(3,33)} = 3.05$, $p = 0.04211$) and significant main effects of Time ($F_{(1,11)} = 32.8$, $p = 0.0001$) and Electrode ($F_{(3,33)} = 9.61$, $p = 0.0001$). Owing to significant interaction between Time × Electrode, a Sidak post hoc analysis of the interaction was performed. Testing shows that there were no differences in CG impedance among electrodes after implantation (0 week; $p \geq 0.05$). At two weeks after implantation, CG impedance significantly increased in all electrodes (E1–E4; $p < 0.0005$). Furthermore, the CG impedance of E3 and E4 (closest to the bladder) was significantly higher than that of E1 and E2 ($p < 0.01$, closest to the spine).

Correlation Between Electrode CG Impedance and Interface Tissue Fibrosis

Increases in CG impedance are often attributed to tissue fibrosis; however, as illustrated in Figure 2c1, the increase in CG impedance

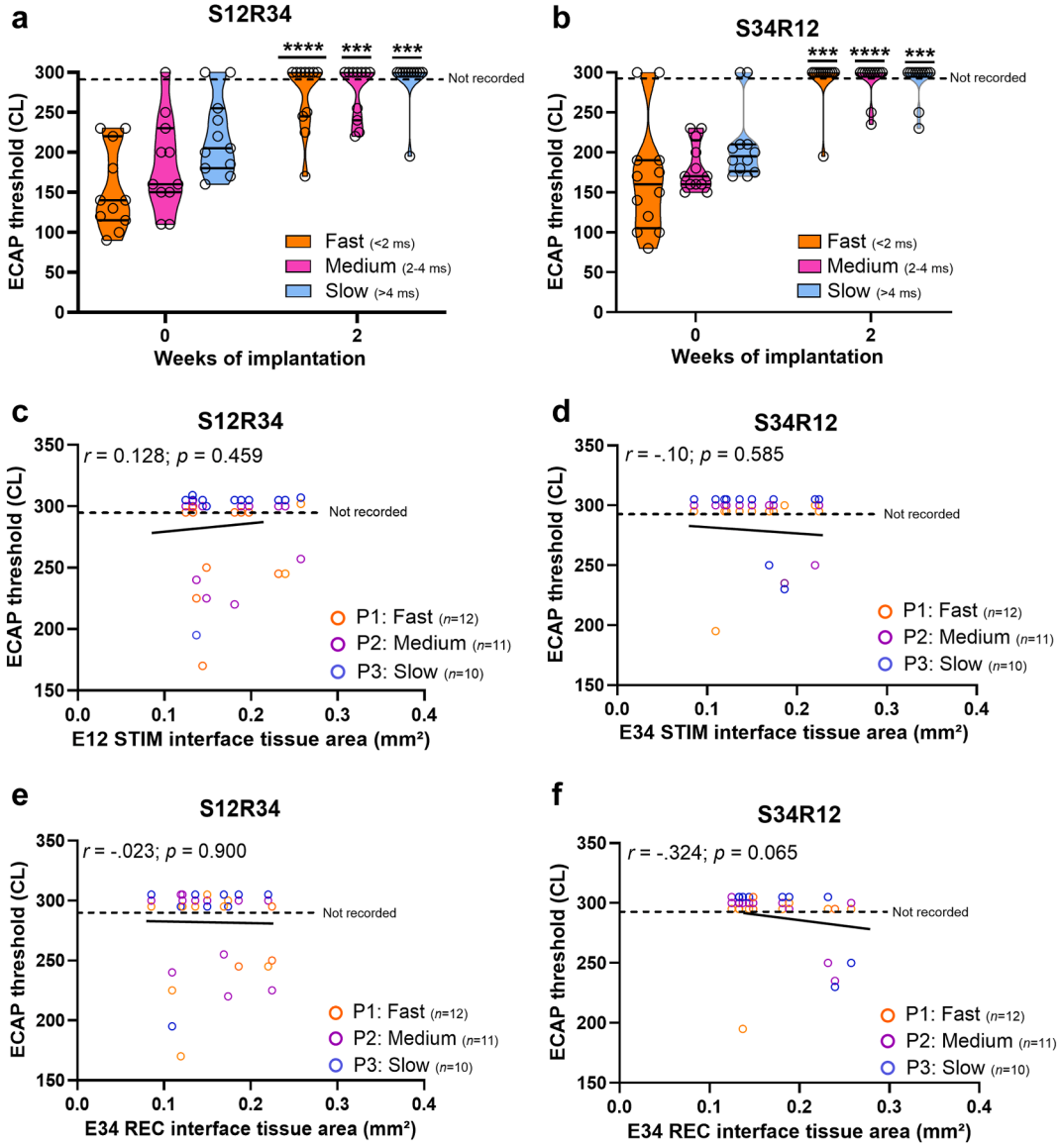

Figure 3. Correlation between ECAP threshold and fibrotic tissue area within the interface after two weeks of pelvic nerve implantation. Panels a and b: After implantation surgery, electrical stimulation evoked three distinct neural populations that had fast (P1: <2 milliseconds), medium (P2: 2–4 milliseconds), and slow (P3: > 4 milliseconds) latency. At two weeks after implantation, ECAP threshold increased compared with the threshold at implantation (week 0, $p < 0.05$), and the recording efficiency decreased across all populations (P1–P3). If responses were not recorded, these data were represented as having a "threshold" of 300 CL (indicated by dotted line, not recorded) for display purposes. Data in panel a indicate evoked responses acquired using an electrode configuration of stimulating E1–E2 and recording E3–E4. Data in panel b indicate evoked responses acquired using electrode configuration of stimulating E3–E4 and recording E1–E2. Panels c and d: Fibrotic tissue area within the stimulating electrode interface had no correlation with change in neural threshold. Panels e and f: Fibrotic tissue area within recording electrode interface had no correlation with whether a response was recorded. Data in the violin graphs in panels a and b show individual values, median ± interquartile range. Significant differences were assessed using a two-way ANOVA and indicated as * $p < 0.05$; ** $p < 0.01$; *** $p < 0.001$; **** $p < 0.0001$. Data in panels c to f show individual pairs, and the correlation between interface tissue area and ECAP threshold was assessed using Pearson's correlation and significance accepted as $p < 0.05$. REC, recording; STIM, stimulation. [Color figure can be viewed at www.neuromodulationjournal.org]

over the two-week implantation period had little to no dependence on fibrotic tissue area. This was confirmed through Pearson's correlation between an electrode's change (Δ) in CG impedance, that is, the net difference between impedance at 0 and two weeks, and the fibrotic tissue area of that same electrode ($r_{(48)} = -0.148$, $p = 0.304$).

Changes in Transimpedance During Long-Term Implantation

Transimpedance was recorded from $N = 7$ rats from a total of 28 electrodes after surgery and after two weeks of long-term implantation on the pelvic nerve. As expected, transimpedance was similar for all electrodes immediately after surgery and appeared relatively stable during the two weeks of implantation (Fig. 2d). A two-way (Time × Electrode) RM ANOVA was performed to analyze the effect of Time × Electrode (E1–E4) on transimpedance. There was no significant interaction between Time × Electrode ($F_{(3,18)} = 0.52$, $p = 0.667$) or Time ($F_{(1,6)} = 0.001$, $p = 0.924$), but Electrode ($F_{(3,15)} = 14.71$, $p < 0.0001$) had a significant effect on transimpedance. Sidak's post hoc analysis on Electrode showed E3 and E4 (distal, closest to bladder) had significantly

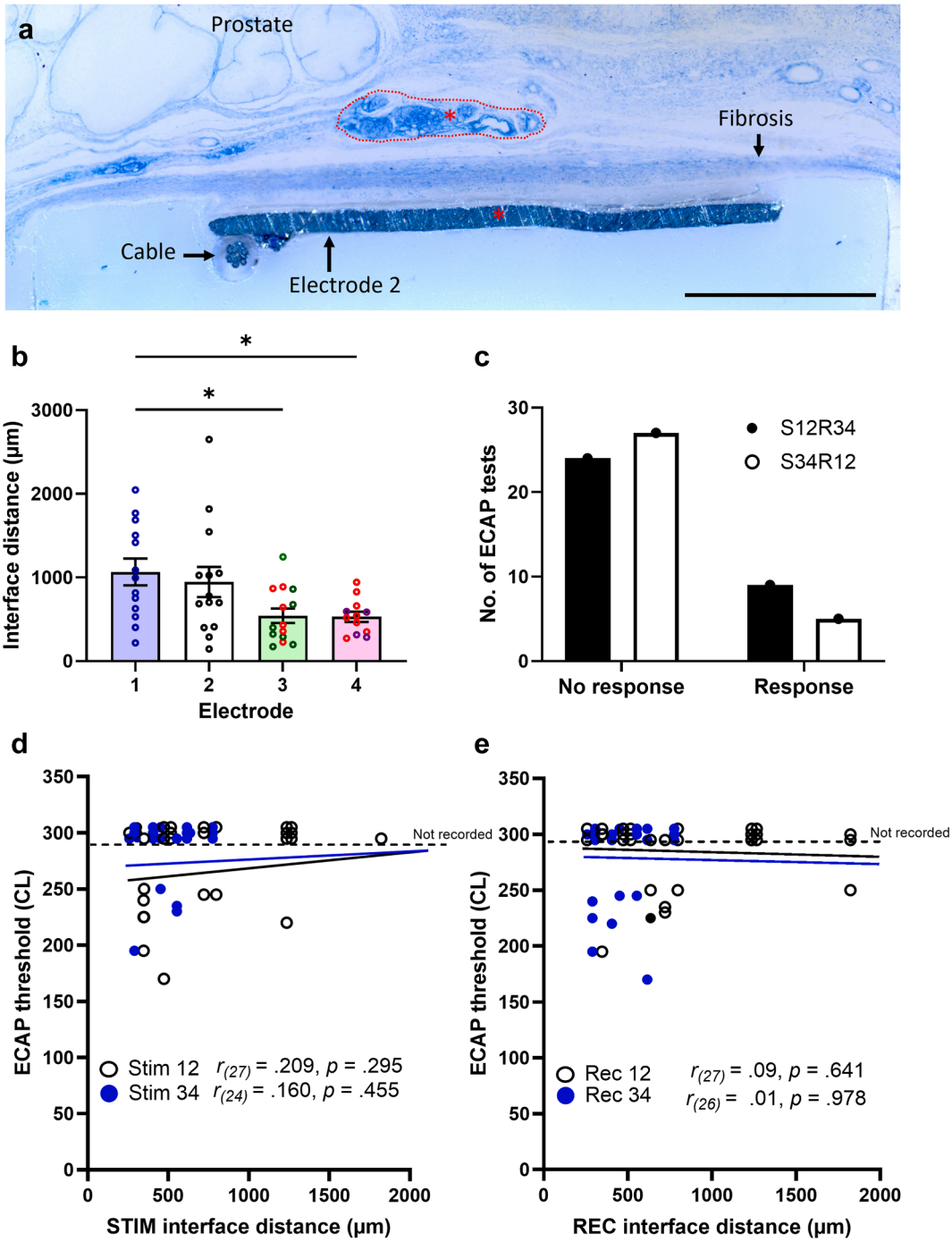

Figure 4. Correlation between the interface and change in ECAP threshold after two weeks of pelvic nerve implantation. The representative image in panel a shows an epoxy-resin embedded Toluidine blue stained sample taken at electrode 2 level and pelvic nerve tissue (outlined by red dotted lines). The distance between the center of the electrode and pelvic nerve (indicated by red *) was measured and correlated with ECAP threshold. b. The distance between neural tissue and the Pt electrode ("interface distance") was assessed across the array (E1–E4). Red circles indicate major pelvic ganglion tissue. c. The number of ECAP tests (N = 12 rats, N = 33 tests) that produced a "response" or "no response" from electrode configurations S12R34 and S34R12. d. The interface distance from stimulating electrodes (S12 and S34) had no correlation with ECAP threshold. e. The interface distance from recording electrodes (R12 and R34) had no correlation with ECAP threshold. Scale bar in panel a represents 1 mm. Data in panel b show individual values, mean ± SEM. Data in panels c and d show individual pairs; the correlation between interface tissue area and ECAP threshold was assessed using Pearson's correlation, and significant differences indicated as * $p < 0.05$. REC, recording; STIM, stimulation. [Color figure can be viewed at www.neuromodulationjournal.org]

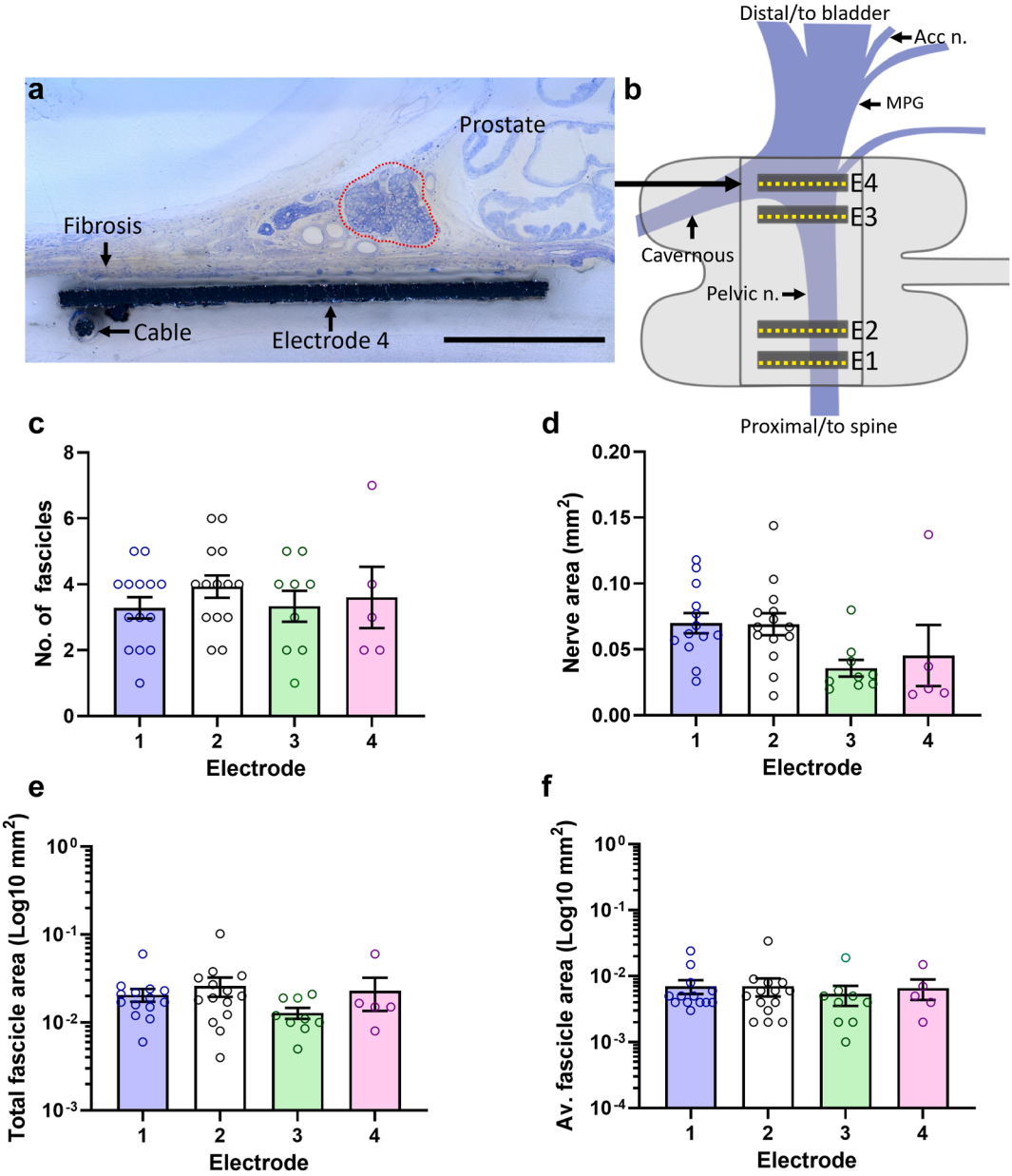

Figure 5. Assessing pelvic nerve morphology in situ after two weeks of pelvic nerve implantation. a. Representative image of block face stained with Toluidine blue at the interface at electrode 3 (distal or closest to the bladder) that includes an MPG (indicated by red dotted line). b. Schematic diagram shows the likely placement of >50% of electrode arrays after two weeks implantation. c. The area of the pelvic nerve (mm^2) (defined as fascicles and blood vessels contained within the boundary of the epineurium) was measured across electrodes 1 to 4. d. The total number of fascicles within the nerve was counted. e. The total area (mm^2) of pelvic nerve fascicles was assessed. f. The average fascicle area (total area/total number of fascicles) was assessed and data on the y-axis displayed as a Log 10 for display purposes. Data in panels c to f show individual values, mean ± SEM. The y-axis in panels e and f is shown as Log10 mm^2. Differences were assessed using RM one-way ANOVA and significant differences indicated as * $p < 0.05$. The scale bar in panel a represents 500 µm. Acc n., accessory nerve; Av., average; MPG, major pelvic ganglion. [Color figure can be viewed at www.neuromodulationjournal.org]

higher transimpedances than did E1 and E2 ($p < 0.001$, proximal), but there were no differences between the nearest adjacent electrodes E1 and E2, or E3 and E4 ($p > 0.05$).

Correlation Between Electrode Transimpedance and Interface Tissue Fibrosis

Increases in transimpedance are often attributed to tissue fibrosis; however, as illustrated in Figure 2d1, the transimpedance after two weeks of implantation was not higher with greater tissue fibrosis. This was confirmed through Pearson's correlation between an electrode's transimpedance, that is, the recorded impedance from the nearest adjacent electrode, and fibrotic tissue area of that same electrode ($r_{(32)} = -0.334$, $p = 0.082$).

ECAP Thresholds

Changes In Neural Threshold During Long-Term Implantation. Similar to that described previously,[11,41] at the time of surgery (week 0), three ECAP waveforms were typically observed in

recording from the pelvic nerve. These had distinct latencies of P1 or "Fast" conduction velocity population (<2 milliseconds), P2 or "Medium" conduction velocity population (2–4 milliseconds), and P3 or "Slow" conduction velocity population (>4 milliseconds).

For both electrode configurations, stimulating E1–E2 and recording from E3–E4 (Stim 12 Rec 34 [S12R34], Fig. 3a) and stimulating E3 to E4 and recording from E1 to E2 (Stim 34 Record [S34R12], Fig. 3b), faster conduction velocity responses were associated with lower thresholds and thresholds increased after two weeks of implantation. A two-way (Time × Neural population) RM ANOVA on S12R34 ECAP thresholds indicated there was no significant interaction between Time × Neural population ($F_{(2,20)} = 2.47$, $p = 0.110$); however, there was a significant main effect of Time ($F_{(1,10)} = 40.2$, $p < 0.0001$) and Neural population ($F_{(2,20)} = 9.49$, $p = 0.0013$).

A similar analysis of S34R12 ECAP thresholds indicated similar results with no significant interaction between Time × Neural population ($F_{(2,15)} = 2.08$, $p = 0.167$) but a significant main effect of Time ($F_{(1,11)} = 138.4$, $p < 0.0001$) and Neural population ($F_{(1.3,14.7)} = 2.0$, $p = 0.178$).

At the time of surgery, the ability to record the three waveforms (P1, P2, P3) or the efficiency of recording was similar when using electrode configuration S12R34 and S34R12. However, after two weeks of implantation, the efficiency of recording with S12R34 decreased to 41.7% for P1, 33.3% for P2, and 8.3% for P3 (Fig. 3a). The efficiency of recording was less with electrode configuration S34R12, with only 8.3% recording of P1, 16.7% of P2, and 16.7% of P3 populations (Fig. 3b).

Correlation Between Change in Neural Threshold and Interface Tissue Fibrosis. Increased tissue fibrosis would be expected to increase neural thresholds by making the stimulation less efficient and/or decreasing the recorded signal strength. However, as illustrated in Figure 3c to f, there was little to no dependence of neural threshold change with fibrotic tissue area, as confirmed by Pearson's correlations (S12Rec34: $r_{(32)} = 0.128$, $p = 0.459$, Fig. 3c; S34R12: $r_{(29)} = -0.10$, $p = 0.585$, Fig. 3d) or recording electrodes (S12Rec34: $r_{(29)} = -0.023$, $p = 0.900$, Fig. 3e; S34R12: $r_{(29)} = -0.324$, $p = 0.065$, Fig. 3f).

Effect of Electrode Interface on the Quality of Extracted Neural Activity

Differences in the Distance Between Neural Tissue and Pt Electrode Across the Array. The distance separating each electrode from the pelvic nerve also was measured from block-face images after Toluidine blue staining. The representative example in Figure 4a shows electrode 2 and the pelvic nerve (outlined by red dotted lines). The distance between the center of the electrode and pelvic nerve (indicated by red *) was measured and correlated with ECAP threshold.

The distance between neural tissue, that being the pelvic nerve and major pelvic ganglia (indicated in Fig. 4b as red circles), and Pt electrode was assessed at each electrode (E1–E4, Fig. 4a). One-way RM ANOVA ($F_{(3,49)} = 4.151$; $p = 0.011$) with Tukey post hoc tests showed distal electrodes 3 (E3, $p = 0.0375$) and 4 (E4, $p = 0.0418$) were significantly closer to neural tissue than distal electrode 1 (E1, closest to the spine). There were no significant differences in interface distance between electrodes 2, 3, and 4 (E2–E4, $p > 0.05$; Fig. 4b).

No Difference in the Efficacy of Recording ECAPs Between Electrode Configurations. Given the shorter electrode-neural distance for E3 and E4 than for E1, we assessed whether the shorter distance improved the ability to record an ECAP (Fig. 4c). Responses from Fast (P1, <2 milliseconds), Medium (P2, 2–4 milliseconds), and Slow (P3, 4–8 milliseconds) fiber were combined for this analysis population ($N = 12$ rats; S12R34: 24 no responses, nine responses; S34R12: 27 no responses, five responses). The relation between these variables was not significant, χ^2 (1, $N = 33$) = 1.30, $p = 0.253$, suggesting an ECAP response was no more likely to be evoked in the S12R34 configuration than in the S34R12 configuration.

No Correlation of the Distance Between Neural Tissue, Pt Electrode, and ECAP Threshold. As illustrated in Figure 4a, neural tissue was in closer proximity to electrodes 3 and 4, ie, shorter interface distance, than to electrodes 1 and 2 (longer interface distance), which may have been expected to decrease neural thresholds. However, as illustrated in Figure 4d,e, the shorter distance had little to no effect on neural thresholds. Pearson's correlations of ECAP threshold and neural distance were not significant when assessing either the stimulating (S12: ($r_{(27)} = 0.209$, $p = 0.295$; S34: $r_{(27)} = 0.160$, $p = 0.455$; Fig. 4d) or recording (R12: $r_{(27)} = -0.034$, $p = 0.868$; R34: $r_{(27)} = -0.006$, $p = 0.978$; Fig. 4e) distance.

Pelvic Nerve Morphology Across the Electrode Array

Migration of the Electrode Array in a Subset of Animals. Block-faced images were assessed at electrodes 1 to 4 (E1–E4, Fig. 5) within $N = 14$ rats. During implantation surgery, there was visual confirmation from the surgeon that all electrodes (E1–E4, Fig. 1a) were placed over the pelvic nerve and not over the major pelvic ganglion. However, after two weeks after implantation, the positioning of most electrode arrays was displaced, causing distal electrodes (E3–E4) to be immediately adjacent to ganglion tissue (Fig. 5a,b). Specifically, 42% of tissue (6/14 samples) within E3 and 57% of tissue (8/14 samples) at E4 showed ganglion tissue at the interface. This was not observed for E1 or E2 in any animal.

Features of the Pelvic Nerve Across the Electrode Array. Owing to the migration of the electrode array over the major pelvic ganglion in some animals, the number of electrodes confirmed to be over the pelvic nerve varied across the array (E1: $N = 14$, E2: $N = 14$, E3: $N = 9$; E4: $N = 5$). We have therefore chosen to report population statistics for each electrode location but have not statistically compared the electrodes.

Number of fascicles: The number of pelvic nerve fascicles across the electrode array ranged from two to seven (E1: two–five fascicles; E2: two–six fascicles; E3: two–five fascicles; E4: two–seven fascicles; Fig. 5c), and the mean number of fascicles was similar across electrodes (E1: 3.3 ± 0.32, E2: 3.9 ± 0.34, E3: 3.33 ± 0.47. 3.6 ± 0.93). Therefore, although it was not possible to trace individual fascicles across the length of the array, there was no evidence of distal branching.

Pelvic nerve area: The mean area of the pelvic nerve (defined as fascicles and blood vessels contained with the boundary of the epineurium) across the electrode array was relatively consistent (E1: 0.07 ± 0.01 mm^2, E2: 0.07 ± 0.01 mm^2, E3: 0.04 ±0.01 mm^2, and E4: 0.05 ± 0.02 mm^2, Fig. 5d), although there was a trend toward less pelvic nerve area more distally.

Total area of pelvic nerve fascicles: The total area of all fascicles within a pelvic nerve was consistent across the array (E1: 0.02 ± 0.003 mm^2, E2: 0.03 ± 0.01 mm^2, E3: 0.01 ± 0.002 mm^2, and E4: 0.02 ± 0.01 mm^2, Fig. 5e).

Average area of pelvic nerve fascicles: Consistent with little change in the total area of pelvic nerve fascicles, the total average

area of individual pelvic nerve fascicles did not vary across the array (E1: 0.007 ± 0.002 mm^2, E2: 0.007 ± 0.002 mm^2, E3: 0.005 ± 0.002 mm^2, and E4: 0.007 ± 0.002 mm^2, Fig. 5f).

DISCUSSION

There is growing interest in using electrical stimulation of the pelvic nerve for the treatment of neuro-urologic and other pelvic functional disorders.[11,31,32] Understanding the impact of the neural tissue–electrode interface is essential for designing suitable peripheral nerve interface electrode arrays and informing on stimulation parameters to advance the future clinical use of pelvic nerve stimulation as a neuromodulation therapy for urologic disorders. In this study, we used a rat pelvic nerve model to investigate ways the characteristics of the "interface," such as the level of fibrosis and distance of the neural tissue from the electrode surface, affect neural activation thresholds when current is delivered through an extraneural electrode.[26] Unexpectedly, this study found no correlation between fibrotic tissue area within the interface and standard clinical measurements of fibrosis (CG impedance, transimpedance) or ECAP thresholds. Interestingly, our results also suggested that the distances of neural tissue from the stimulating electrode and from the recording electrode are equally important in recording an ECAP.

In this study, block-face imaging of histologically stained tissue at the interface was adapted from a previous study[33] and optimized to allow analysis of the interface between implanted electrodes and pelvic neural tissue in situ. Traditional histology techniques in paraffin blocks of implanted tissue are limited because the electrode array must be removed from the tissues before processing, risking damage of the delicate tissues at the electrode interface.[23] There also are limitations of conventional microtome sectioning in regions containing metal of the Pt electrodes.[33] In contrast, block-face imaging enables embedding of both tissue and implanted electrode arrays still intact and applying a grinding technique to erode the surface to allow block-face imaging of serial sections across the electrode array. This technique was originally developed for in situ observation of the placement of cochlear implant electrodes relative to cochlear anatomy.[17,34,42] To achieve this, the conventional protocol used to assess the bony structures of the cochlear was adapted for the soft delicate tissues of the eye to assess safety and placement of a retinal implant that was secured epiretinally with a metal tack.[33] In this study, for what we believe is the first time, we adapted the epoxy resin embedding, grinding, polishing, and imaging under various magnifications for the soft prostate and connected pelvic neural tissues to allow a reliable assessment of the neural tissue interface.

CG impedance significantly increased at all electrodes (E1–E4) at two weeks after implantation, which accords with our previous observations of impedance increases after eight weeks of long-term implantation on the pelvic nerve using the same device.[11] Similar increases in impedance are reported after four to five weeks of implantation on other autonomic nerves, such as the abdominal vagus nerve of rats.[7,8] Interestingly, transimpedance showed no changes over time. However, transimpedance measurements were sensitive to electrode placement in the body because higher transimpedances were observed in distal electrodes (E3, E4) than in proximal (E1, E2). CG impedance is the measure of peak voltage at the end of the stimulation phase and is dominated by the effects of the current passing through the stimulating electrode. CG impedance is therefore most sensitive to changes in the stimulating electrode (eg, biofouling, corrosion, etc). In comparison, the transimpedance matrix, sometimes referred to as the "Stimulation-Current-Induced Non-Stimulating Electrode Voltage recording,"[24] measures the voltage on adjacent unstimulated electrodes. When removing the confounding issue of the voltage induced from polarizing stimulating electrode, the voltage readings on unstimulated electrodes more likely reflect the surrounding environment and have been used clinically to identify mispositioning of cochlear implants.[24] Electrochemical impedance spectrometry can be used to thoroughly assess impedance at a large range of frequencies[43] and can provide additional information compared with the simpler pulse-based CG and transimpedance measurements used in this study.[44] However, the scope of the study was restricted to assessing impedance measurements performed with commercially available devices routinely used clinically.

After implantation of an electrode array around an autonomic nerve, benign epineural scar tissue is generally formed over two weeks.[45] Inflammation due to array implantation typically causes leukocyte adhesion, cytokine and chemokine release, neurovascularization, and fibroblast formation, contributing to fibrosis or scar tissue at the interface.[23] In this study, interface tissue fibrosis was generally uniform across all electrodes. However, despite this uniformity of fibrosis across electrode interfaces, CG impedance of E3 and E4 (distal) was higher than in E1 and E2 (proximal), even though there was no correlation between tissue fibrotic area and impedance. One explanation might be the tissue underneath the nerve near the distal electrodes E3–E4 (as an example, E4 in Fig. 1b). The different density of prostate tissue and fatty tissues (Fig. 2a shows E2) likely contributed to the impedance measures. Taken together, we conclude that neither CG impedance nor transimpedance reliably detects the amount of fibrotic tissue at the interface.

It is interesting to note that higher CG impedance and transimpedance were detected on E3 and E4 than on E1 and E2, despite the distance between neural tissue and the Pt electrode surface of E3–E4 being shorter than that of E1–E2. Our data suggest CG impedance also was affected by other unknown factors within the interface. Measuring interface fibrotic tissue area does not consider the density of the fibrotic tissue, with denser tissue likely to have a larger effect on impedance than less dense fibrotic tissue.[23] Other factors, such as the physical properties of Pt electrodes, including corrosion, pitting, dissolution, or damage, can lead to an increase in electrode surface area and a subsequent decrease in impedance.[21] However, these changes to electrode physical properties are usually observed after application of high levels of charge during long-term stimulation, and given these electrodes received minimal stimulation (<10 min/wk during ECAP testing for two weeks), this is an unlikely explanation. Electrode biofouling, which involves the accumulation of biological matter (protein deposits, cells, etc) at the electrode-electrolyte interface, is another well-known factor that causes the reduction of the effective active electrode area and subsequent increase in electrical impedance.[22,23] Furthermore, electrical stimulation (130 Hz, 60–μs pulse width, 80–100 μA: rat dependent) can readily disrupt the deposited monolayer of adsorbed protein on the electrode surface to effect impedances in long-term implanted deep brain stimulation electrodes.[46] As such, CG impedance also may have been affected by other unknown factors within the interface. ECAP thresholds significantly increased over two weeks of implantation, and the ability to record an ECAP response concurrently decreased.

There were no differences in recording efficiency among S12R34 and S34R12 configurations, and no correlation between the distance of neural tissue from stimulating or recording electrodes. This suggests the interface distance of stimulating and recording electrodes equally affects the recording of an ECAP.

At the time of surgical implantation, the four-electrode array was placed over the pelvic ganglion, as confirmed visually. Block-face imaging of long-term implanted devices revealed that the placement of >50% of arrays had moved during the two-week implantation period so that distal electrodes were directly adjacent to ganglion tissue. Electrode array migration also occurs in other neuromodulation technologies (eg, spinal cord electrode migration occurs at 2.1% to 27%[47,48] and often causes loss of treatment efficacy and the need for additional corrective surgery).[49] However, electrode migration can be reduced by anchoring technologies and surgical technique,[50] or for the current neural target, shortening the array.

In conclusion, electrode impedance and neural thresholds can indicate the presence of fibrotic tissue but do not specifically inform on the amount of fibrotic tissue within the interface. Understanding the electrode-nerve interface is essential for designing efficacious electrode arrays to advance the future clinical use of neuromodulation therapy for urologic disorders.

Acknowledgements

The authors acknowledge Ms Amy Morley, Ms Philippa Kammerer, and Mr Jerico Matarazzo for laboratory and technical assistance. They also acknowledge Ms Chiara Braida and Ms Lisa Dyball for histologic processing and analysis of block-face imaging samples.

Data Availability

The data that support the findings of this study will be openly available after an embargo at the following https://doi.org/10.5061/dryad.xgxd254tm.

Ethics Statement

This animal study was approved by St. Vincent's Hospital Animal Research and Ethics Committee—approval: 12/19.

Authorship Statements

All authors listed have made a substantial, direct, and intellectual contribution to the work. Sophie C. Payne provided expertise in urogenital anatomy and electrical impedance and was involved in conceptualization, data curation, formal analysis, experimental design/methods, project administration, supervision (equal), and original draft manuscript writing—review and editing. Christopher Bowman was involved in data curation, formal analysis, project administration, and manuscript writing—review and editing. Janet R. Keast provided knowledge in urogenital anatomy and was involved in conceptualization, experimental design, formal analysis, and manuscript writing—review and editing. Ella P. Trang provided expertise in block face imaging techniques and input in formal analysis, histology methods, and manuscript writing—review and editing. Peregrine B. Osborne provided knowledge in urogenital anatomy and was involved in conceptualization, experimental design, formal analysis, data curation, and manuscript writing—review and editing. James B. Fallon provided knowledge in electrical engineering and was involved in conceptualization, data curation, formal analysis, experimental design/methods, project administration, supervision, and original draft manuscript writing—review and editing. Janet R. Keast (principal investigator), Peregrine B. Osborne, and James B. Fallon (coinvestigators) provided funding for the experimental activities (OT2OD023872). All authors approved the final revised manuscript.

Conflict of Interest

The authors reported no conflict of interest.

How to Cite This Article

Payne S.C., Bowman C., Keast J.R., Trang E.P., Osborne P. B., Fallon J.B. 2025. Correlation of Electrical Impedance and Evoked Potentials With Properties of the Electrode Interface Using in Situ Block-Face Imaging of the Rat Pelvic Nerve.
Neuromodulation 2025; ■: 1–12.

REFERENCES

1. Cracchiolo M, Ottaviani MM, Panarese A, et al. Bioelectronic medicine for the autonomic nervous system: clinical applications and perspectives. *J Neural Eng*. 2021;18:1002. https://doi.org/10.1088/1741-2552/abe6b9.
2. Huang J, Fan Y, Zhao K, et al. Comparative efficacy of neuromodulation technologies for overactive bladder in adults: a network meta-analysis of randomized controlled trials. *Neuromodulation*. 2023;26:1535–1548. https://doi.org/10.1016/j.neurom.2022.06.004.
3. Waltz E. A spark at the periphery. *Nat Biotechnol*. 2016;34:904–908. https://doi.org/10.1038/nbt.3667.
4. Davis CJ, Musselman ED, Grill WM, Pelot NA. Fibers in smaller fascicles have lower activation thresholds with cuff electrodes due to thinner perineurium and smaller cross-sectional area. *J Neural Eng*. 2023;20: 026032. https://doi.org/10.1088/1741-2552/acc42b.
5. Peña E, Pelot NA, Grill WM. Computational models of compound nerve action potentials: efficient filter-based methods to quantify effects of tissue conductivities, conduction distance, and nerve fiber parameters. *PLoS Comput Biol*. 2024;20: e1011833. https://doi.org/10.1371/journal.pcbi.1011833.
6. Leblans M, Sismono F, Vanpoucke F, et al. Novel impedance measures as biomarker for intracochlear fibrosis. *Hear Res*. 2022;426: 108563. https://doi.org/10.1016/j.heares.2022.108563.
7. Payne SC, Furness JB, Burns O, et al. Anti-inflammatory effects of abdominal vagus nerve stimulation on experimental intestinal inflammation. *Front Neurosci*. 2019;13:418. https://doi.org/10.3389/fnins.2019.00418.
8. Payne SC, Romas E, Hyakumura T, Muntz F, Fallon JB. Abdominal vagus nerve stimulation alleviates collagen-induced arthritis in rats. *Front Neurosci*. 2022;16: 1012133. https://doi.org/10.3389/fnins.2022.1012133.
9. Payne SC, Ward G, Fallon JB, et al. Blood glucose modulation and safety of efferent vagus nerve stimulation in a type 2 diabetic rat model. *Physiol Rep*. 2022;10: e15257. https://doi.org/10.14814/PHY2.15257.
10. Payne SC, Burns O, Stebbing M, et al. Vagus nerve stimulation to treat inflammatory bowel disease: a chronic, preclinical safety study in sheep. *Bioelectron Med*. 2018;1:235–250. https://doi.org/10.2217/bem-2018-0011.
11. Payne SC, Wiedmann NM, Eiber CD, et al. Recording of electrically evoked neural activity and bladder pressure responses in awake rats chronically implanted with a pelvic nerve array. *Front Neurosci*. 2020;14: 619275. https://doi.org/10.3389/fnins.2020.619275.
12. Ahmed U, Chang Y-C, Lopez MF, et al. Implant- and anesthesia-related factors affecting cardiopulmonary threshold intensities for vagus nerve stimulation. *J Neural Eng*. 2021;18: 046075. https://doi.org/10.1088/1741-2552/ac048a.
13. Wu C, Evans JJ, Skidmore C, Sperling MR, Sharan AD. Impedance variations over time for a closed-loop neurostimulation device: early experience with chronically implanted electrodes. *Neuromodulation*. 2013;16:46–50 [discussion: 50].

14. Sillay KA, Rutecki P, Cicora K, et al. Long-term measurement of impedance in chronically implanted depth and subdural electrodes during responsive neurostimulation in humans. *Brain Stimul*. 2013;6:718–726. https://doi.org/10.1016/j.brs.2013.02.001.
15. Brummer SB, McHardy J, Turner MJ. Electrical stimulation with Pt electrodes: trace analysis for dissolved platinum and other dissolved electrochemical products. *Brain Behav Evol*. 1977;14:10–22. https://doi.org/10.1159/000124611.
16. Brummer SB, Turner MJ. Electrochemical considerations for safe electrical stimulation of the nervous system with platinum electrodes. *IEEE Trans Bio Med Eng*. 1977;24:59–63. https://doi.org/10.1109/TBME.1977.326218.
17. Tykocinski M, Duan Y, Tabor B, Cowan RS. Chronic electrical stimulation of the auditory nerve using high surface area (HiQ) platinum electrodes. *Hear Res*. 2001;159:53–68. https://doi.org/10.1016/S0378-5955(01)00320-3.
18. Clark GM, Shute SA, Shepherd RK, Carter TD. Cochlear implantation: osteoneogenesis, electrode-tissue impedance, and residual hearing. *Ann Otol Rhinol Laryngol Suppl*. 1995;166:40–42.
19. Grill WM, Mortimer JT. Electrical properties of implant encapsulation tissue. *Ann Biomed Eng*. 1994;22:23–33. https://doi.org/10.1007/BF02368219.
20. Huang CQI, Tykocinski M, Stathopoulos D, Cowan R. Effects of steroids and lubricants on electrical impedance and tissue response following cochlear implantation. *Cochlear Implants Int*. 2007;8:123–147. https://doi.org/10.1179/cim.2007.8.3.123.
21. Shepherd RK, Carter PM, Enke YL, et al. Chronic intracochlear electrical stimulation at high charge densities: reducing platinum dissolution. *J Neural Eng*. 2020;17: 056009. https://doi.org/10.1088/1741-2552/abb7a6.
22. Harris AR, Carter P, Cowan R, Wallace GG. Impact of protein fouling on the charge injection capacity, impedance, and effective electrode area of platinum electrodes for bionic devices. *ChemElectroChem*. 2021;8:1078–1090.
23. Gold MR, Van Veldhuisen DJ, Hauptman PJ, et al. Vagus nerve stimulation for the treatment of heart failure: the INOVATE-HF trial. *J Am Coll Cardiol*. 2016;68:149–158. https://doi.org/10.1016/j.jacc.2016.03.525.
24. Klabbers TM, Huinck WJ, Heutink F, Verbist BM, Mylanus EAM. Transimpedance matrix (TIM) measurement for the detection of intraoperative electrode tip fold-over using the slim modiolar electrode: a proof of concept study. *Otol Neurotol*. 2021;42:e124–e129. https://doi.org/10.1097/MAO.0000000000002875.
25. Grill WM, Pelot NA. Computational modeling of autonomic nerve stimulation: Vagus et al. *Curr Opin Biomed Eng*. 2024;32: 100557. https://doi.org/10.1016/j.cobme.2024.100557.
26. Hussain MA, Grill WM, Pelot NA. Highly efficient modeling and optimization of neural fiber responses to electrical stimulation. *Nat Commun*. 2024;15:7597. https://doi.org/10.1038/s41467-024-51709-8.
27. Eiber CD, Payne SC, Biscola NP, et al. Computational modelling of nerve stimulation and recording with peripheral visceral neural interfaces. *J Neural Eng*. 2021;18: 066020. https://doi.org/10.1088/1741-2552/ac36e2.
28. Bertrand MM, Keast JR. Dissection of pelvic autonomic ganglia and associated nerves in male and female rats. *J Vis Exp*. 2020;157:10–3791. https://doi.org/10.3791/60904.
29. Bertrand MM, Korajkic N, Osborne PB, Keast JR. Functional segregation within the pelvic nerve of male rats: a meso- and microscopic analysis. *J Anat*. 2020;237:757–773. https://doi.org/10.1111/joa.13221.
30. Pelot NA, Behrend CE, Grill WM. Modeling the response of small myelinated axons in a compound nerve to kilohertz frequency signals. *J Neural Eng*. 2017;14: 046022. https://doi.org/10.1088/1741-2552/aa6a5f.
31. Crook JJ, Brouillard CBJ, Irazoqui PP, Lovick TA. Chronic implantation of cuff electrodes on the pelvic nerve in rats is well tolerated and does not compromise afferent or efferent fibre functionality. *J Neural Eng*. 2018;15: 024001. https://doi.org/10.1088/1741-2552/aaa569.
32. Peh WYX, Mogan R, Thow XY, et al. Novel neurostimulation of autonomic pelvic nerves overcomes bladder-sphincter dyssynergia. *Front Neurosci*. 2018;12:186. https://doi.org/10.3389/fnins.2018.00186.
33. Nayagam DAX, Durmo I, McGowan C, Williams RA, Shepherd RK. Techniques for processing eyes implanted with a retinal prosthesis for localized histopathological analysis: part 2 epiretinal implants with retinal tacks. *J Vis Exp*. 2015;96: e52348. https://doi.org/10.3791/52348.
34. Shepherd R, Verhoeven K, Xu J, Risi F, Fallon J, Wise A. An improved cochlear implant electrode array for use in experimental studies. *Hear Res*. 2011;277:20–27. https://doi.org/10.1016/j.heares.2011.03.017.
35. Matarazzo JV, Williams-Wynn DT, Fallon JB, Payne SC. Magnetically coupled percutaneous connector for chronic electrical peripheral nerve stimulation and recording in awake rats. *IEEE Trans Bio Med Eng*. 2025;72:35–42. https://doi.org/10.1109/TBME.2024.3436649.
36. Fallon JB, Payne S, R Keast J, B Osborne P. Implantation of a pelvic nerve array in rats. Accessed October 21, 2020. https://www.protocols.io/view/implantation-of-a-pelvic-nerve-array-in-rats-14egn85myg5d/v1.
37. Fallon JB, Senn P, Thompson AC. *A highly configurable neurostimulator for chronic pre-clinical stimulation studies. Paper presented at: Neural Interfaces Conferences, June 25-27, 2018*. Minneapolis, MN; 2018.
38. Fallon JB, Payne SC. Electrophysiological recording of electrically-evoked compound action potentials. Accessed October 21, 2020. https://www.protocols.io/view/electrophysiological-recording-of-electrically-evo-yxmvmxmp9l3p/v1.
39. Guedes MC, Brito Neto RVB, Gomez MVSG, et al. Neural response telemetry measures in patients implanted with Nucleus 24®. *Braz J Orl*. 2005;71:660–667. https://doi.org/10.1016/S1808-8694(15)31271-4.
40. Schindelin J, Arganda-Carreras I, Frise E, et al. Fiji: an open-source platform for biological-image analysis. *Nat Methods*. 2012;9:676–682. https://doi.org/10.1038/nmeth.2019.
41. Payne SC, Osborne PB, Thompson A, Eiber CD, Keast JR, Fallon JB. Selective recording of physiologically evoked neural activity in a mixed autonomic nerve using a minimally invasive array. *APL Bioeng*. 2023;7: 046110. https://doi.org/10.1063/5.0164951.
42. Briggs RJS, Tykocinski M, Xu J, et al. Comparison of round window and cochleostomy approaches with a prototype hearing preservation electrode. *Audiol Neurootol*. 2006;11:42–48. https://doi.org/10.1159/000095613.
43. Hazelgrove B, Matter L, Raos B, et al. Electrochemical impedance spectroscopy in vivo for neurotechnology and bioelectronics. *Nat Rev Electr Eng*. 2025;2:110–124. https://doi.org/10.1038/s44287-024-00126-6.
44. Dalrymple AN, Huynh M, Nayagam BA, et al. Electrochemical and biological characterization of thin-film platinum-iridium alloy electrode coatings: a chronic in vivo study. *J Neural Eng*. 2020;17: 036012. https://doi.org/10.1088/1741-2552/ab933d.
45. Larson CE, Meng E. A review for the peripheral nerve interface designer. *J Neurosci Methods*. 2020;332: 108523. https://doi.org/10.1016/j.jneumeth.2019.108523.
46. Evers J, Sridhar K, Liegey J, Brady J, Jahns H, Lowery M. Stimulation-induced changes at the electrode–tissue interface and their influence on deep brain stimulation. *J Neural Eng*. 2022;19: 046004.
47. North RB, Recinos VR, Attenello FJ, Shipley J, Long DM. Prevention of percutaneous spinal cord stimulation electrode migration: a 15-year experience. *Neuromodulation*. 2014;17:670–676 [discussion: 676]. https://doi.org/10.1111/ner.12151.
48. Gupta M, Abd-Elsayed A, Hughes M, Rotte A. A retrospective review of lead migration rate in patients permanently implanted with percutaneous leads and a 10 kHz SCS device. *Pain Res Manag*. 2021;2021: 6639801. https://doi.org/10.1155/2021/6639801.
49. Dombovy-Johnson ML, D'Souza RS, Ha CT, Hagedorn JM. Incidence and risk factors for spinal cord stimulator lead migration with or without loss of efficacy: a retrospective review of 91 consecutive thoracic lead implants. *Neuromodulation*. 2022;25:731–737. https://doi.org/10.1111/ner.13487.
50. Hayek SM, Veizi E, Hanes M. Treatment-limiting complications of percutaneous spinal cord stimulator implants: a review of eight years of experience from an Academic Center Database. *Neuromodulation*. 2015;18:603–608 [discussion: 608]. https://doi.org/10.1111/ner.12312.